The Structure of the Mineral Chestermanite, $Mg_{2.25}Al_{0.16}Fe_{0.43}Ti_{0.02}Sb_{0.13}O_2BO_3$. A Combined Single-Crystal X-Ray and HREM Study

V. Alfredsson,[a] J.-O. Bovin,[a] R. Norrestam[b,*] and O. Terasaki[a,†]

[a]National Center for HREM, Chemical Center, University of Lund, P.O. Box 124, S-221 00 Lund and [b]Department of Structural Chemistry, Arrhenius Laboratory, University of Stockholm, S-106 91 Stockholm, Sweden

Alfredsson, V., Bovin, J.-O., Norrestam, R. and Terasaki, O., 1991. The Structure of the Mineral Chestermanite, $Mg_{2.25}Al_{0.16}Fe_{0.43}Ti_{0.02}Sb_{0.13}O_2BO_3$. – Acta Chem. Scand. 45: 797–804.

The crystal structure of the borate mineral chestermanite, $Mg_{2.25(4)}Al_{0.16(2)}Fe_{0.43(5)}Ti_{0.02(1)}Sb_{0.13(1)}O_2BO_3$, from the Twin Lakes region in California, has been studied by single-crystal X-ray diffraction and electron microscopy techniques. Chestermanite has been verified to be a member of the pinakiolite family of minerals, and its structure is isotypic with that of orthopinakiolite. The X-ray study, based on the non-diffuse reflections, indicates an orthorhombic space group, *Pbam*, with unit cell parameters $a = 18.525(4)$, $b = 12.272(2)$ and $c = 3.0218(4)$ Å and $Z = 8$. The structural model has been refined versus the 2539 most significant X-ray reflections with $\sin\theta/\lambda \leq 1.10$ Å^{-1} to an R-value of 0.043.

Electron energy-loss spectra (EELS) recorded in a transmission electron microscope with a parallel EELS detector unveiled magnesium, iron, oxygen and boron in the crystals of chestermanite. The composition obtained by the X-ray study, $(Mg,Al)_{2.494(3)}(Fe,Ti)_{0.386(3)}Sb_{0.120(1)}O_2BO_3$, agrees reasonably well with that found (cf. above) by EDX analysis, viz. $(Mg,Al)_{2.41(4)}(Fe,Ti)_{0.45(5)}Sb_{0.13(1)}O_2BO_5$, on the selected crystal.

The main source for the occurrence of diffuse super-lattice reflections observed in the electron diffraction patterns of chestermanite can qualitatively be explained by a simple extended structural model that takes account of an ordering of the mixed metal ion content (Sb and Mg/Al) at one of the metal positions.

Dedicated to Professor Sten Andersson on the occasion of his 60th birthday.

The mineral chestermanite was reported by Erd and Ford[1] from a small brucite marble body in the Twin Lakes region in California, as grayish green crystals. Its crystal structure is isotypic with that of orthopinakiolite (cf. Takéuchi *et al.*)[2] and its reported composition is $Mg_{2.28}Al_{0.20}Fe_{0.38}Sb_{0.12}Ti_{0.02}BO_5$. Chestermanite belongs to the pinakiolite family of minerals, with the general formula $M_3O_2BO_3$. M can be both divalent as Mg^{2+}, Mn^{2+}, Fe^{2+}, Co^{2+} or Ni^{2+} and/or trivalent as Mn^{3+}, Fe^{3+} and Al^{3+}, but also tetra- and pentavalent as Sn^{4+}, Ti^{4+} and Sb^{5+}.

The structures of the members of the pinakiolite family can be considered as built up by chemical twinning[3] of the parent structure of pinakiolite (or hulsite) as presented by Takéuchi.[4] The oxygen coordination around the metal ions is octahedral, and such octahedra are linked together by corner- and edge-sharing to form flat walls, F walls, and zig-zag walls. With the notation of Takéuchi, the central columns of octahedra through the zig-zag walls are denoted C walls and those at the corners of these walls S columns. The first twin member of the family, ludwigite, has two layers of octahedra between the twin planes and is denoted -2t2t2t2-. The second member, orthopinakiolite or chestermanite, has the twin sequence -4t4t4t4-. Two more members, tekéuchiite and blatterite, with the sequences -6t6t6t6- and -8t8t8t8-, are known. Several members of the family, e.g. the synthetic ludwigite $Co_3O_2BO_3$, are potential catalysts as judged from preliminary tests on total combustions of hydrocarbons.

Structural investigations of a synthetic Mg–Mn orthopinakiolite (Norrestam *et al.*, to be published) and of the minerals takéuchiite,[5] blatterite[6] and a new Sb-rich variant of pinakiolite,[7] have shown that the presence of considerable amounts of Mn^{3+} causes structural disorder. This is apparently due to effects of the Jahn–Teller type, which cause every second Mn^{3+}-free layer in the C wall to show positional disorder of the metal ions. Chestermanite is the first -4t4t4t4- structure known that has no Mn^{3+} content, and its structure can be expected to be a good representative of a non-distorted basic structure of the -4t4t4t4- type.

*To whom correspondence should be addressed.

† On leave from: Department of Physics, Tohoku University, Aramaki Aoba, Sendai 980, Japan.

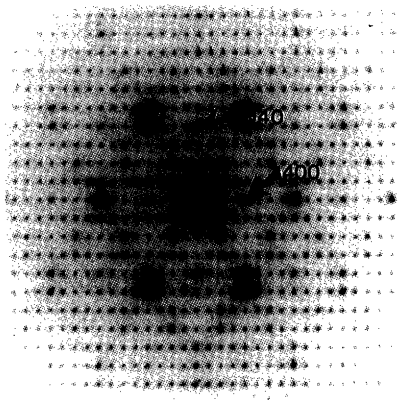

Fig. 1. Selected-area diffraction pattern recorded with the beam along [001] of the selected crystal (used for the X-ray diffraction studies) of chestermanite.

Experimental

Electron microscopy studies. Crystal fragments of the mineral were collected on a holey carbon film supported on a copper grid for preliminary studies. The electron microscope used was a JEM-4000EX, operated at 400 keV and capable of performing studies with a structural resolution better than 1.6 Å, as verified by optical diffraction of electron micrographs. Selected area electron diffraction (Fig. 1), recorded along [001], verified that all of the crystals belonged to the -4t4t4t4- type of the pinakiolite family. The corresponding structure images (Fig. 2) confirmed this observation.

For further microscopy studies, the crystal used for the X-ray diffraction data collection was retained. It was dismounted from the glass needle and transferred to a JSEM-840A scanning electron microscope (SEM) equipped with a LINK AN10000 energy-dispersive X-ray (EDX) detector. The EDX spectra [Fig. 3(d)] were processed by the computer programs ZAF-4/FLS.[8]

The crystal used for X-ray data collection was dismounted from the SEM holder and crushed between two glass plates. The fragments were collected onto a holey carbon film and transferred to a JEM-2000FX electron microscope equipped with a LINK AN10000 system for EDX analysis. In order to verify the existence of oxygen and boron in the single crystal used for X-ray studies and in other crystal fragments of the chestermanite mineral, an electron energy-loss (EELS) investigation was performed. Such work had not previously been performed on oxyborates of the pinakiolite family. The EELS spectra were recorded with a Gatan (M666) parallel detection spectrometer at 160 kV in a JEM-2000Fx transmission electron microscope. The LaB_6 electron emission filament was run with an emission current of 1 μA. A spectrometer entrance aperture of 1 mm was used into image mode. The energy scale was calibrated against spectra recorded for NiO and BN crystals. The oxygen and boron edges could be recorded (Fig. 3), in addition to the edges of magnesium and iron.

Selected-area diffraction (SAED) patterns in different directions revealed disorder along the *c*-axis. The SAED shown in Fig. 4 was recorded along [100] and also shows higher-order Laue zones (HOLZ) 1 and 2. The reflections *hkl* with $l = 1/2$ are diffuse. The diffuse intensity can be seen up to the next HOLZ [Fig. 4(b)]. In some directions the diffuse scattering is more concentrated in spots than in other cases [Figs. 4(c) and 5]. The diffuse reflections with $l = 1/2$ are in general considerably weaker than the well defined ones with integer values of *l*. Thus, the X-ray diffraction study, which is based on non-diffuse reflections with integer *l* (giving a subcell with a *c*-axis of 3.02 Å) will only give a basic average structure. The observations of the *h*00 and 0*k*0 reflections with *h* odd and *k* odd in the electron diffraction pattern shown in Fig. 1 are not compatible with the space-group symmetry *Pbam*. However, the occurrence of these reflections can probably be ascribed to dynamical (multiple) scattering effects, as they almost disappear on

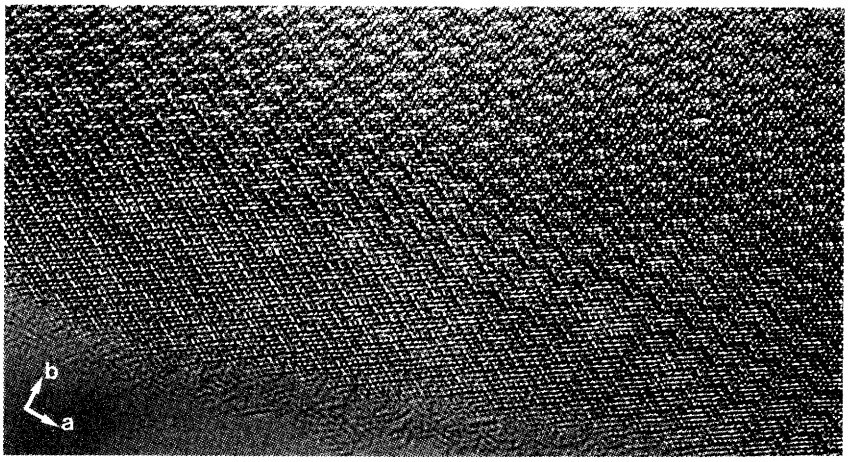

Fig. 2. High-resolution electron micrograph (JEM-4000EX microscope) of the selected crystal (used for the X-ray diffraction studies) of chestermanite with the beam parallel to the *c*-axis.

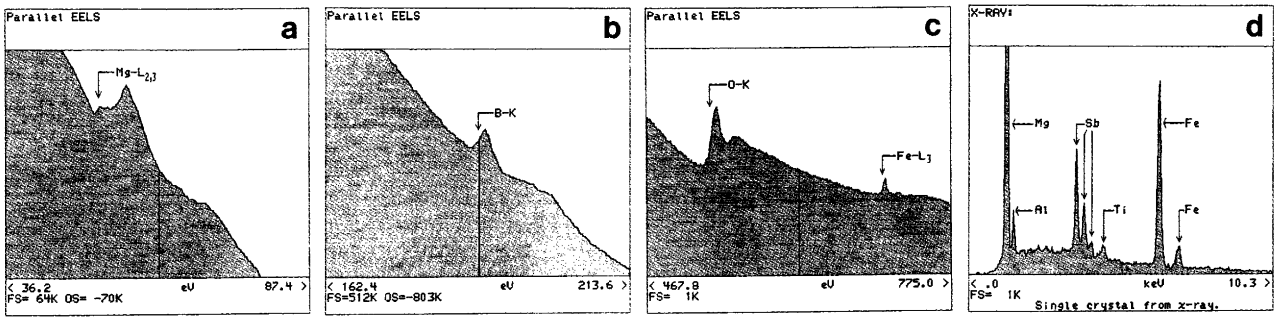

Fig. 3. Electron energy-loss spectra, EELS, recorded from thin fragments of chestermanite crystals, showing EELS edges for (a) magnesium, (b) boron and (c) iron. The energy dispersive X-ray spectrum (EDS) from the single crystal used for the crystal structure determination is shown in (d).

tilting the crystal along the b^*-axis [Fig. 4(c)]; the diffuse intensity on the b^*-axis [Fig. 4(c)] may not be genuine for the same reasons.

High-resolution images (Fig. 6) were recorded from the same crystal to permit a comparison with the basic average structure derived from the X-ray diffraction study. The computer-simulated image inserted in the figure was calculated with the atomic positions and occupancies obtained from the X-ray study (discussed below). The calculations were performed with a local IBM PS/2-80 version of the SHRLI software package[9] using the following microscope parameters: spherical aberration constant 1.0 mm, semi-angle of beam convergence 0.25 mrad, focus −470 Å, half width of spread of gaussian focus 30 Å and beam tilt 6.4 mrad towards [110].

X-ray diffraction studies. X-ray diffraction photographs, using de Jong and precession techniques, indicated the possible space group symmetries *Pbam* or *Pba2*. The centrosymmetric space group *Pbam*, tentatively adopted in the present study, was supported by the outcome of the structural refinements. The crystal X-ray diffraction data collected with a single-crystal diffractometer were corrected for background, Lorentz, polarization and absorption effects. Details of the experimental conditions and of the final structural refinements are listed in Table 1.

The initial atomic coordinates for *Pbam* symmetry were derived from those obtained by Takéuchi *et al.*[2] for the lower *Pnnm* symmetry of their orthopinakiolite specimen. Chestermanite contains ions of Mg, Al, Fe, Sb and a rather negligible amount of Ti. Owing to the similarities of the X-ray scattering powers of Mg and Al on the one hand and of Fe and Ti on the other, the structural refinements were

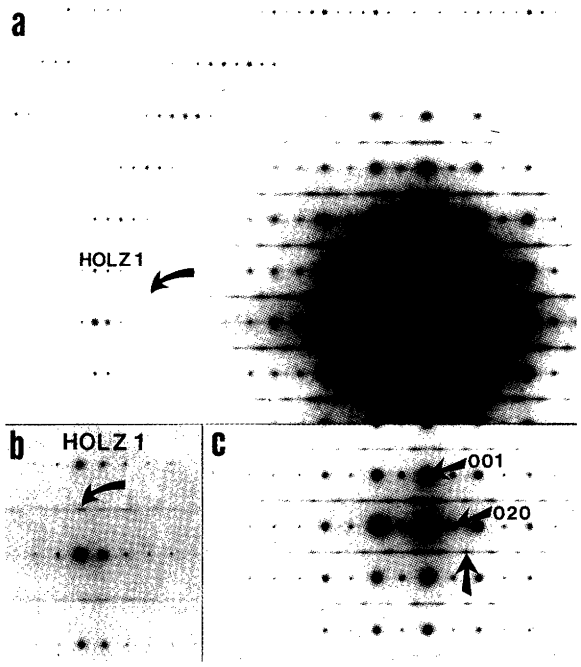

Fig. 4. Selected-area electron diffraction (SAED) patterns of the selected crystal (used for the X-ray diffraction studies) of chestermanite recorded along the *a*-axis. The higher-order Laue zones (HOLZ) 1 and 2 are visible. The diffuse scattering (cf. arrows in the figures) half-way between the principle spots (in the *c*-direction) makes up planes, as they are seen also in HOLZ 1 [Fig. 4(b)]. The diffuse scattering is concentrated in spots which do not follow the extinction rules for the space group used in the X-ray study.

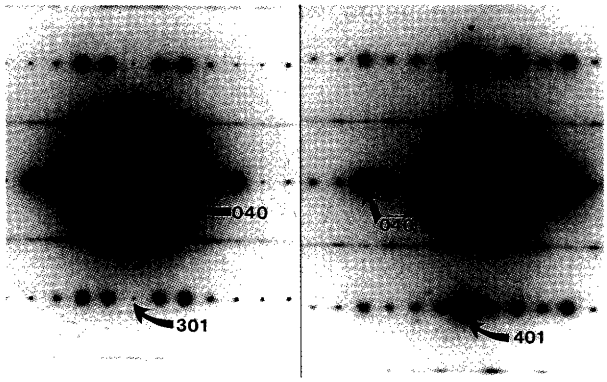

Fig. 5. SAED patterns from the selected crystal (used for the X-ray diffraction studies) of chestermanite showing that the diffuse scattering is, in some directions, more concentrated into spots.

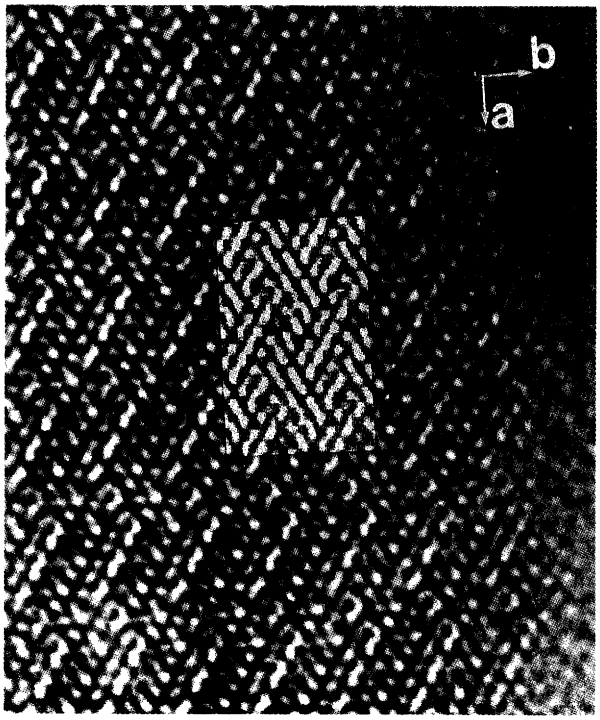

Fig. 6. HREM crystal structure image of the chestermanite crystal used in the X-ray study. The image was recorded along [001] at Scherzer focus and with 400 keV (JEM-4000EX). The inserted image is a computer simulation, using the atomic coordinates from the X-ray diffraction study. The image is recorded with the crystal slightly tilted towards [110]. The tilt is taken into account in the simulated image.

carried out using only the scattering factors of the elements Mg and Fe to describe the metal content at the different metal positions. Accordingly, the relative amounts of Mg

Table 2. Fractional atomic coordinates ($\times 10^4$) and thermal parameters ($\times 10^4$ Å^2) for the chestermanite structure.[a]

Atom	*x*	*y*	*z*	U_{eq}
M(1)	0	0	0	56(1)
M(2)	0	5000	0	87(2)
M(3)	1247(1)	1708(1)	5000	81(2)
M(4)	1275(1)	3893(1)	0	82(1)
M(5)	2570(1)	2710(1)	0	75(1)
M(6)	3746(1)	1089(1)	5000	84(2)
M(7)	3728(1)	3885(1)	5000	86(2)
O(1)	686(1)	317(1)	5000	96(2)
O(2)	629(1)	2472(2)	0	86(2)
O(3)	702(1)	4629(2)	5000	124(3)
O(4)	1991(1)	1266(1)	0	92(2)
O(5)	1834(1)	3137(1)	5000	121(3)
O(6)	3117(1)	313(1)	0	88(2)
O(7)	3208(1)	2454(1)	5000	107(2)
O(8)	3006(1)	4321(1)	0	85(2)
O(9)	4507(1)	1525(1)	0	91(2)
O(10)	4500(1)	3474(1)	0	90(2)
B(1)	−115(1)	2513(2)	0	82(3)
B(2)	2373(1)	293(2)	0	80(3)

Atom	U_{11}	U_{22}	U_{33}	U_{12}
M(1)	56(1)	57(1)	56(1)	1(1)
M(2)	69(3)	87(3)	106(3)	−14(3)
M(3)	81(3)	78(3)	84(3)	− 8(2)
M(4)	87(2)	60(2)	99(3)	2(1)
M(5)	64(2)	76(2)	86(2)	− 4(1)
M(6)	87(3)	75(3)	90(3)	9(2)
M(7)	83(3)	83(3)	93(3)	− 8(2)

[a]The equivalent isotropic thermal parameters (U_{eq}) of the metal atoms were estimated at 1/3 Tr (*U*). The anisotropic temperature factor expression (space group symmetry *Pbam*) used for the metal atoms is:

$$\exp[-2\pi^2((ha^*)^2U_{11} + (kb^*)^2U_{22} + (lc^*)^2U_{33} + 2hka^*b^*U_{12})].$$

Table 1. Experimental conditions for the crystal structure determination of chestermanite.

Formula (from EDS on crystal)	$Mg_{2.25}Al_{0.16}Fe_{0.43}Ti_{0.02}Sb_{0.13}O_2BO_5$
Formula weight (a.m.u.)	190.6
Space group	*Pbam*
Unit cell dimensions	$a = 18.525(4)$, $b = 12.272(2)$, $c = 3.0218(4)$ Å
Unit cell volume, *V*	687.0(2) Å^3
Formula units per unit cell, *Z*	8
Calculated density, D_x	3.69 g cm^{-3}
Radiation	Mo *K*α
Wavelength, λ	0.71073 Å
Temperature, *T*	293(1) K
Crystal shape	Prismatic
Crystal size	0.10 × 0.04 × 0.34 mm
Diffractometer	Enraf–Nonius CAD4
Determination of unit cell:	
Number of reflections used	17
θ-range	12.5 to 15.8°
Intensity data collection:	
Maximum sin(θ)/λ	1.10 Å^{-1}
Range of *h*, *k* and *l*	0–40, 0–26 and 0–6
Standard reflections	2
Intensity instability	<3 %
Internal *R* value	0.031
No. of unique reflections	425
No. of observed reflections	2539
Criterion for significance	$I > 5\sigma(I)$
Absorption correction:	
Linear absorption coefficient	28.5 cm^{-1}
Transmission factor range	0.76–0.89
Structure refinement:	
Minimization of	$\Sigma w\Delta F^2$
Anisotropic thermal parameters	All metal atoms
Isotropic thermal parameters	B and O atoms
No. of refined parameters	79
Weighting scheme	$(\sigma^2(F) + 0.0004\|F\|^2)^{-1}$
Final *R*	0.043
Final *wR*	0.053
Final $(\Delta/\sigma)_{max}$	0.03
Final $\Delta\varrho_{min}$ and $\Delta\varrho_{max}$	−2.5 and 2.1 e Å^{-3}

Table 3. Metal composition (e.s.d.s 0.4 %) at the metal sites as obtained in the structural refinements, metal–oxygen distances in the coordination octahedra and bond multiplicities.[a]

Composition	Atoms	Distance	Multiplicity
48.2 % Sb + 51.8 % MgAl	M(1)–O(1)	2.013	4
	O(10)	2.090	2
24.4 % FeTi + 75.6 % MgAl	M(2)–O(3)	2.045	4
	O(9)	2.084	2
100 % MgAl	M(3)–O(1)	1.999	1
	O(2)	2.116	2
	O(4)	2.116	2
	O(5)	2.063	1
18.9 % FeTi + 81.1 % MgAl	M(4)–O(2)	2.116	1
	O(3)	2.057	2
	O(5)	2.053	2
	O(6)	2.076	1
46.0 % FeTi + 54.0 % MgAl	M(5)–O(4)	2.072	1
	O(5)	2.102	2
	O(7)	1.945	2
	O(8)	2.137	1
100 % MgAl	M(6)–O(3)	2.064	1
	O(6)	2.132	2
	O(7)	1.950	1
	O(9)	2.135	2
100 % MgAl	M(7)–O(1)	2.066	1
	O(7)	2.003	1
	O(8)	2.087	2
	O(10)	2.142	2
	B(1)–O(2)	1.378	
	O(9)	1.373	
	O(10)	1.405	
	B(2)–O(4)	1.388	
	O(6)	1.379	
	O(8)	1.385	

[a]Owing to the similarities in the X-ray scattering powers of Mg and Al and of Fe and Ti, MgAl and FeTi denote unknown compositions of these pairs of atom types. The bond length e.s.d.s are 0.002 Å for metal–oxygen and 0.003 Å for boron–oxygen bonds.

to Al and of Fe to Ti, as determined by the EDX analysis (cf. above), could not be verified by the X-ray investigation. The final atomic coordinates, metal occupancies and thermal parameters are given in Table 2. The metal compositions at the different metal positions and relevant metal–oxygen bond lengths are listed in Table 3. Despite the neglect of the diffuse scattering clearly visible on the SAED patterns (cf. above), the *R*-value of 0.043 is satisfactorily low and supports the relevance of the structural model derived for the basic average structure.

The structural refinements were performed by means of the SHELX-76 package[10] using scattering factors for neutral atoms from Ref. 11. The polyhedral packing diagrams were obtained with the computer graphics program POLY.[12]

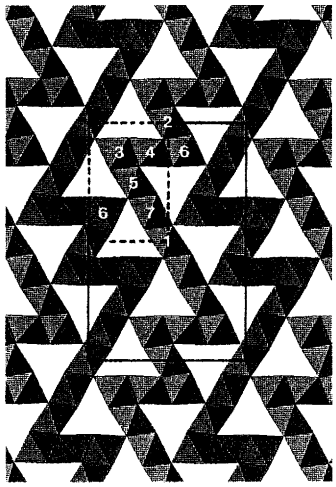

Fig. 7. Polyhedral drawing of the chestermanite structure (orthopinakiolite type) viewed along the *c*-axis. The unit cell and the atom numbering (Table 2) used for the metal positions are indicated. The boron atoms (not shown) occupy the trigonal voids in the structure. The *b*-axis is horizontal, the *a*-axis is vertical and the origin is at the upper left corner.

Structural results

The derived model of the structure of chestermanite (Fig. 7) agrees in general with that of the previous study[2] of the Mn^{3+}-containing orthopinakiolite, apart from the lower symmetry (*Pnnm*) and doubled *c*-axis of the latter structure. As discussed above, the chestermanite (or orthopinakiolite) structure can be derived from that of the simple pinakiolite (Fig. 8) by considering a twinning model. Chestermanite contains flat walls (F walls) which are seven octahedra wide and zig-zag walls. The C walls, consisting of the central octahedra through the zig-zag walls, are five octahedra wide. The F walls (Fig. 9) consist of columns of octahedra around the metal positions M(3), M(5), M(7) and M(1). Owing to the inversion centre at the M(1) posi-

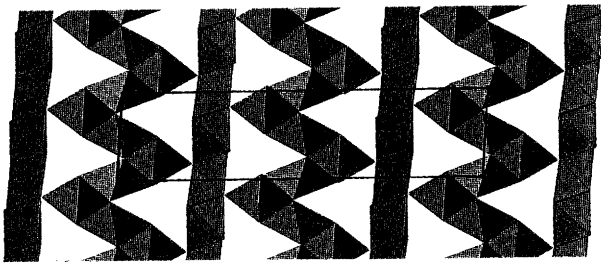

Fig. 8. Polyhedral drawing of an example of the pinakiolite structure,[7] a Sb-rich pinakiolite from Långban, Sweden. Boron atoms are not shown. The *a*-axis (21.773 Å) is horizontal, the *b*-axis (5.327 Å) is vertical and the origin is at the upper left corner. The monoclinic structure ($\beta = 94.38°$), with space group symmetry *C2/m* is viewed along the *c*-axis (6.153 Å). By combining slabs of two units of pinakiolite and relating them by glide-plane symmetry, the structure of chestermanite (Fig. 2) can be deduced.

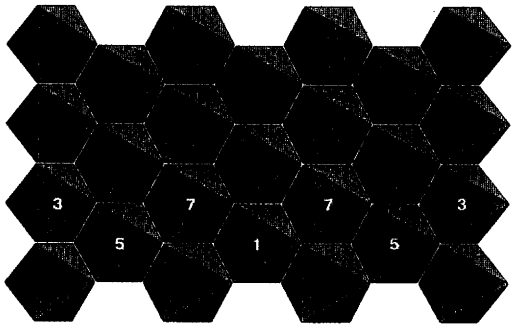

Fig. 9. Polyhedral drawing of the flat F wall in chestermanite, viewed perpendicular to the wall. The numbering of the metal positions (Table 2) in the wall is indicates. The *c*-axis is vertical.

tion, the F walls become seven columns wide, with the sequence of metal positions in the columns M(3)–M(5)–M(7)–M(1)–M(5)–M(3). Similarly, the C walls (Fig. 10) consist of the five columns of octahedra in the sequence M(5)–M(4)–M(2)–M(4)–M(5), as the M(2) position is also at an inversion centre.

The structural refinements showed M(1) to be the only metal position with an Sb content (48.2 %). The short M(1)–O bond lengths (Table 3), average 2.038 Å, indicate pentavalent rather than trivalent Sb. This is also supported by a calculation of the empirical bond valence at the metal position, 3.46, using a linear combination of the parameter values given by Brown and Altermatt.[13] This value is in agreement with the formal charge, +3.45, calculated for 48.2 % Sb^{5+} and 51.8 % Mg^{2+}. The metal–oxygen bond length distributions (cf. Shannon),[14] as well as bond-valence calculations, suggest that the iron ions are trivalent.

The distribution of metal ions (Table 3), 48.2 % Sb^{5+} at M(1), 46.0 % Fe^{3+} at M(5) and no Sb^{5+} or Fe^{3+} at the M(3) and M(7) positions would give alternating metal ion charges, 2.00–2.46–2.00–3.45–2.00–2.46–2.00 (the low amount of Al^{3+} being neglected), between the columns M(3)–M(5)–M(7)–M(1)–M(7)–M(5)–M(3) of the F wall. The corner columns of the zig-zag wall, the S columns, are

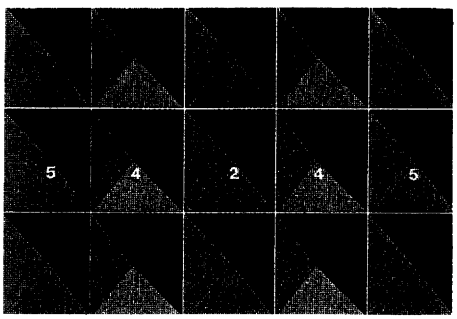

Fig. 10. Polyhedral drawing of the central octahedral columns, the C wall, through the zig-zag wall viewed perpendicular to the wall. The numbering of the metal positions (Table 2) in the wall is indicated. The *c*-axis is vertical.

formed by the octahedra around M(3), also terminal columns of the F wall, and around M(6). None of these columns has any Fe^{3+} content, and the metal ion charge is probably low (low Al^{3+} content), as the bond valences are as low as 2.08 and 2.09. Such distributions of the metal ion charges in the F walls and in the S columns are in agreement with those found in other pinakiolites, such as takéuchiite.[5]

The B–O distances in the borate groups range from 1.373(3) to 1.388(3) Å, except for the B(1)–O(10) distance of 1.405(3) Å. This elongation is possibly due to coulomb effects, since O(10) is the only borate oxygen atom that also coordinates the highly charged (+3.45) M(1) metal ion containing pentavalent Sb.

All the thermal parameters (Table 2) appear to have physically reasonable values. The largest ones are, as expected, obtained for the oxygen atoms O(1), O(3), O(5) and O(7), which are not constituents of any of the borate groups. All the oxygens, except for the O(3) and O(5) atoms, are tetrahedrally coordinated by metal ions. The five-coordinated (roughly a square pyramid) oxygens O(3) and O(5) have the highest thermal parameters of any of the atoms. Bond valences calculated for the oxygen positions range from 1.87 to 2.04, in reasonable agreement with the formal charge of −2.00.

The mean value of six EDX spectra collected at different points of the selected crystal gave the chemical composition $Mg_{2.25(4)}Al_{0.16(2)}Fe_{0.43(5)}Ti_{0.02(1)}Sb_{0.13(1)}O_2BO_3$, which can be written $(Mg,Al)_{2.41(4)}(Fe,Ti)_{0.45(5)}Sb_{0.13(1)}BO_5$ if elements with similar atomic numbers are combined. The composition obtained from the X-ray structure determination was $(Mg,Al)_{2.494(3)}(Fe,Ti)_{0.386(3)}Sb_{0.120(1)}BO_5$. Thus these two estimates of the composition are in good agreement and also agree with the composition $(Mg,Al)_{2.48}(Fe,Ti)_{0.40}Sb_{0.12}BO_5$ found by Erd and Ford[1] for the mineral specimen.

Diffuse scattering model

With the structural results obtained from the X-ray study, a model can be derived to explain the occurrence of the diffuse scattering observed on the electron diffraction patterns (see e.g. Fig. 4). The main observations of diffuse scattering are shown in Fig. 11(a), which is a schematic drawing of the observed electron diffraction pattern given in Fig. 4(c). The characteristic features are that diffuse reflections are observed for $0kl$ with half-integer values of l, and the positions of the intensity maxima occur at k = odd, while all other reflections are sharp. No intensities are observed for the $00\frac{1}{2}$ and 010 reflections. The diffuse reflections are caused by spatial modulation of the atomic arrangement due to small atomic displacements and/or ordering. The latter case seems to be dominating, as the intensity of the diffuse reflections decreases monotonically from the centroid position. In view of the differences in scattering powers it is reasonable to assume that the metal ordering is the main source of the observed diffuse scattering for the $0kl$ reflections with half-integer l.

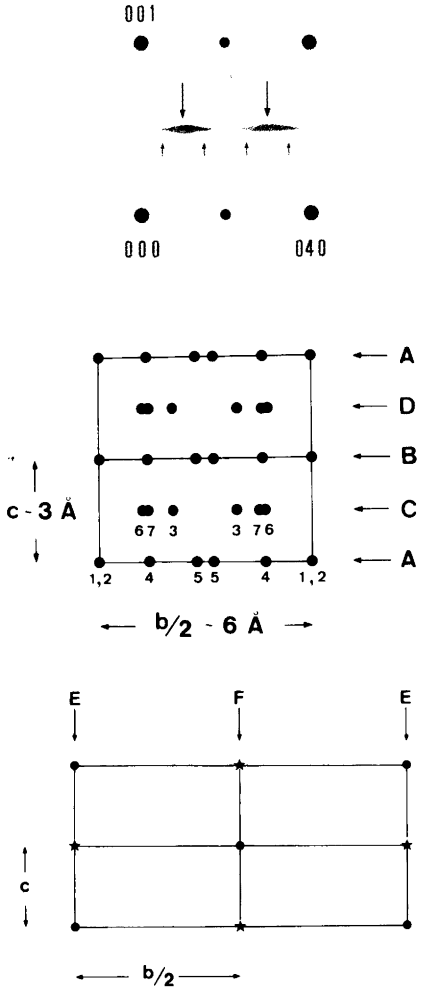

Fig. 11. (a) Schematic drawing of the main features of the observed electron diffraction pattern given in Fig. 4(c). (b) Projection along [100] of the metal atom positions found by the X-ray study. (c) Simplified structure model with two types of scatterers denoted by circles and crosses, respectively. The arrangements in the two planes labelled E and F are antiphase along [001]. The planes are arranged in an ordered way, with a separation of *b*/2 along [010], to give the sequence EF...

Fig. 11(b) shows a projection along [100] of the metal ion positions found by the X-ray study. As no intensity was observed for the $00\frac{1}{2}$ reflection, the total scattering from each of the planes denoted A and B in Fig. 11(b) must be equal, and similarly for each of the two planes denoted C and D.

Fig. 11(c) shows a simplified structural model, where the period along [001] is 2*c* owing to the presence of two types of scatterers (denoted by a star and a circle, respectively) in the structure. If the two scatterers were identical a well defined diffraction pattern consisting of only sharp reflections would of course be obtained. On the other hand, if the scatterers were different, the atomic arrangement would give rise to superlattice reflections for *l* half-integer, as the *c*-axis became doubled.

The model shown in Fig. 11(c) can be described as an arrangement of the EF type, where the letters denote the two ways in which atoms are arranged in planes separated by *b*/2 [Fig. 11(c)]. Such a model structure, with the unit translation *b* along [010], can be described by the sequence EF... and would give superlattice reflections at the positions marked by the large arrows in Fig. 11(a). A structure model with a longer sequence such as EEFF.. (unit translation of 2*b*) would give reflections at the positions marked with the smaller arrows.

In the case where the crystal is built up by domains with a sequence of the EF... type, sequences like EEF, FFE and EEFF can occur at the domain boundaries, depending the type of plane (E or F) at the end and at the start of the domains. The existence of such domains in a structure will give diffuse intensity contributions for half-integer *l* and odd *k* but will not affect the sharp reflections such as 020. The obtained intensity distribution of the diffuse reflections will be dependent on the domain sizes. Thus, the model suggested that consists of domains each with the sequence ..EF.. can explain the occurrence of the observed diffuse reflections in the diffraction patterns.

The remaining problem is to find a reasonable spatial modulation of the ordering of the atomic arrangement at the different metal positions in the chestermanite structure. With reference to Fig. 11(b), the metal positions M(3), M(6) and M(7) can be ignored, as they contain 100 % Mg (Al) and could not give any larger intensity contribution; furthermore, as for the positions M(4) and M(5), the distances along [010] would be different from *b*/2 as is demanded by the model. Of the two remaining positions M(1) and M(2), the latter position is occupied by two different scatterers with the ratio 3:1, and a simple model, giving a metal ordering with unit translation of *c*, is not possible. Therefore, the most probable candidate would be the M(1) position, as the scatterers at this position have a ratio close to 1:1. The difference in scattering powers between the two types of scatterers, Sb and Mg (Al), at this position further supports the conclusion that the main source for the occurrence of diffuse scattering is due to an ordering of the Sb and Mg (Al) content at the M(1) position, by analogy with the 'EF model' [Fig. 11(c)], within domains of the structure.

Acknowledgements. Dr. R. C. Erd, US Geological Survey, California, is greatfully acknowledged for providing the samples. The Swedish National Science Research Council are to be thanked both for the grants to one of the authors (O.T.) to hold a position as a visiting professor and for their support of the research program on metal borates. The availability of the JEM-4000EX, JEM-2000FX and JSEM-840A electron microscopes was made possible through grants from the Alice and Knut Wallenberg Foundation and the Swedish National Science Research Council. This work was also supported by grants from the Swedish National Board of Technical Developments. Mr. L. Thell is acknowledged for his assistance with the image computer simulations.

References

1. Erd, R. C. and Ford, E. E. *Can. Mineral. 26* (1987) 911.
2. Takéuchi, Y., Haga, N., Kato, T. and Miura, Y. *Can. Mineral. 16* (1978) 475.
3. Andersson, S. and Hyde, B. *J. Solid State Chem. 9* (1974) 92.
4. Takéuchi, Y. *Recent Prog. Nat. Sci. Jpn. 3* (1978) 153.
5. Norrestam, R. and Bovin, J.-O. *Z. Kristallogr. 181* (1987) 135.
6. Bovin, J.-O., Norrestam, R., Sjövall, R., Søtofte, I. and Thomasson, R. *Z. Kristallogr. In press.*
7. Norrestam, R. and Hansen, S. *Z. Kristallogr. 191* (1990) 105.
8. Statham, P. J. *Anal. Chem. 49* (1977) 2149.
9. O'Keefe, M. A. and Buseck, P. *Trans. Am. Crystallogr. Assoc. 15* (1979) 27.
10. Sheldrick, G. M. *SHELX-76.* University of Göttingen, FRG 1976.
11. *International Tables for X-Ray Crystallography*, Kynoch Press, Birmingham 1974, Vol. IV.
12. Norrestam, R. *Acta Crystallogr., Sect. A 40* (1984) C-43.
13. Brown, I. D. and Altermatt, D. *Acta Crystallogr., Sect. B 41* (1985) 244.
14. Shannon, R. D. *Acta Crystallogr., Sect. A 32* (1976) 751.

Received December 3, 1990.